Solar Energy Materials & Solar Cells 224 (2021) 111008

Contents lists available at ScienceDirect

Solar Energy Materials and Solar Cells

journal homepage: http://www.elsevier.com/locate/solmat

A recalculation of the efficiency limit in crystalline Si/Si tandem solar cells

F.-J. Haug *, C. Ballif

Ecole Polytechnique Fédérale de Lausanne (EPFL), Institute of Microengineering (IMT), Photovoltaic and Thin-Film Electronics Laboratory, Rue Maladière 71b, CH, 2000, Neuchâtel, Switzerland

ARTICLE INFO

Keywords:
Crystalline silicon
Tandem solar cell
Efficiency limit

ABSTRACT

We determine the limiting efficiency for monolithic tandem solar cells that employ crystalline silicon for the top-cell as well as for the bottom cell. In such a design, the top-cell extends over the region of very high generation rate that forms at the front of the device. Consequently, the design benefits from a high excess carrier density in the top-cell, resulting in a voltage in the tandem device that is more than twice the voltage of equally thick single junction solar cells. Considering Coulomb-enhanced Auger recombination coefficient, we find a maximum efficiency of 30.7% for a total device thickness of 500 μm wherein the top cell thickness amounts to 2.15 μm, representing gain of 1.1% (abs) with respect to the limiting efficiency of single junction devices.

1. Introduction

In 1961, Schockley and Queisser presented a rigorous determination of the limiting efficiency of single junction solar cells with respect to the bandgap [1]. Based on detailed balance, they assumed radiative transitions as only fundamental recombination process and reported an efficiency limit of 30% for the bandgap value of silicon. In 1984, Tiedje calculated the limiting efficiency of silicon solar cells, taking into account the indirect nature of its bandgap as well as Auger recombination [2]. For a cell thickness w, they expressed the $j(V)$ characteristics by $j = j_L - qwR$. The recombination rate R contains the applied bias voltage through the np product which is given by $np = (n_0 + \Delta n)(p_0 + \Delta n) = n_i^2 \exp(qV/kT)$. For R, they used the free-particle parameters of Auger recombination, for j_L they implemented a simplified Lambertian model, and they separated the contributions of band-to-band transitions and of free carrier absorption. Thus, they found an optimum efficiency of 29.8% for a 100 μm thick cell. Also in 1984, Green obtained the same value of 29.8% for a 100 μm thick cell based on an idealized model for current generation and transport; based on diffusive transport within the device, he obtained a practical efficiency limit of 25% for the wafer quality available at the time.

In 2002, Kerr proposed a parametrisation of Coulomb enhanced Auger recombination [3]. Calculating j_L with a ray-tracing approach, they found an optimum efficiency of 29.05% for a 90 μm thick cell of lowly doped material [4]. In 2006, Swanson gave a critical assessment how to bridge the gap between the idealized and the practical efficiency limit, putting the latter at 27% [5]. In 2012, Richter presented an updated parametrisation for Auger recombination [6]. Including the effects of band gap narrowing on n_i^2 [7] but sticking to the simplified optical model of Tiedje, they found an optimum efficiency of 29.43%. for a 110 μm thick cell [8]. In 2018, Schäfer extended Richter's results by a rigorous treatment of Lambertian scattering and found an optimum efficiency of 29.56%. for a 98 μm thick cell [9]. Also in 2018, Veith-Wolf proposed a different Auger parametrisation for n-type silicon which extrapolates to a lower bulk lifetime in lowly doped material; using the same Lambertian scattering model as Schäfer [9], they find an optimum efficiency of 29.47% [10]. In 2019, Bhattacharya proposed an optical design for photocurrents beyond the Lambertian limit, resulting in limiting efficiencies up to 31.07% [11].

Even though silicon solar cells are limited by Auger recombination, we note that the limitation is not due to particularly high Auger coefficients (for example, those of GaAs are even higher [12]). Nevertheless, Auger recombination dominates because the indirect bandgap of silicon yields a very low radiative recombination coefficient and a very weak absorption. Thus, silicon solar cells need thick absorbers that spread the photogeneration over large volumes. As a result, the splitting of the quasi Fermi levels remains moderate and the voltage low compared to the bandgap. To avoid this issue, Green proposed monolithically integrated Si/Si tandem with a matched current density of 21.1 mA/cm^2 [13]. Based on the optimum thickness of single junction cells, he modelled a 100 μm thick device, projected the generation rates within current matched cells of 1.6 μm and 98.4 μm thickness, and used the free-particle Auger model to determine the component voltages under Voc conditions. Finally, using an empiric relation between V_{oc} and

* Corresponding author.
E-mail address: franz-josef.haug@epfl.ch (F.-J. Haug).

https://doi.org/10.1016/j.solmat.2021.111008
Received 2 November 2020; Received in revised form 20 January 2021; Accepted 10 February 2021
Available online 20 February 2021

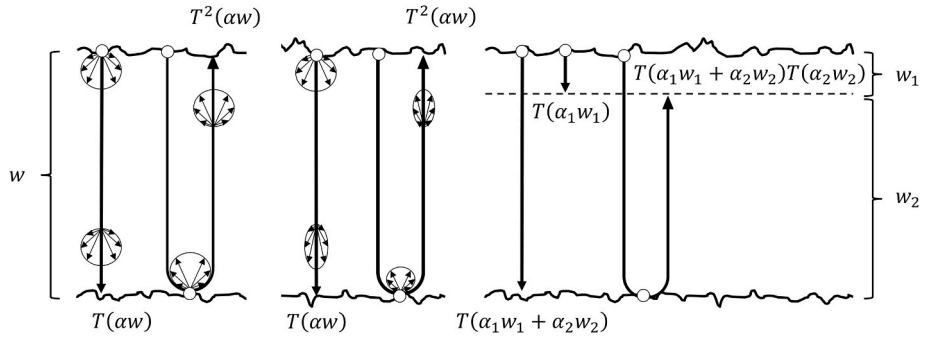

Fig. 1. Fraction of transmitted light between a scattering event (circle) and incidence at an interface (arrowhead). Weakly absorbed light maintains the angular distribution (left), for strongly absorbed light it sharpens until randomisation at the next interface (middle). The right panel illustrates a situation with different absorption coefficients above and below an interconnecting junction.

FF [14], he estimated a limiting efficiency of 30.8% for the tandem device [13].

In this contribution, we revisit the idea of a Si/Si tandem cell. We use current matching at the maximum power point (MPP) without the restriction to a single device thickness, considering band gap narrowing and Coulomb enhanced Auger recombination [6,10,15], and we take into account Lambertian light scattering with photon recycling.

2. Methodology

Our approach assumes a monolithic series-connection and follows the derivation of the efficiency limit of silicon single junction solar cells [2,4,8,9]. Thus, we calculate the $j(V)$ characteristics according to $j(V) = j_L - qwR$ by setting a bias voltage V and solving $np = (n_0 + \Delta n)(p_0 + \Delta n) = n_i^2 \exp(qV/kT)$ for the resulting excess carrier density Δn. Here, the intrinsic carrier density n_i depends on Δn due to band gap narrowing [7]. Next, we assess the absorbtance $A(\lambda)$ which determines the photocurrent j_L, but also the probability for photon recycling P_{PR}. To this end, we assume zero reflection at the front, full randomisation by Lambertian light scattering, attenuated propagation across the cell thickness w as described by a transmission term $T(\alpha w)$, and perfect rear reflection. Upon its return to the front, light arriving within the escape-cone is coupled out, the remainder is subject to total internal reflection. For a single-junction device, multiple round-trips yield an infinite sum which is readily evaluated to the following expression [16]:

$$A(\lambda) = \frac{\alpha_{bb}}{(\alpha_{bb} + \alpha_{FCA})} \cdot \frac{(1 - T(\alpha w)) + T(w)(1 - T(\alpha w))}{1 - T^2(\alpha w)(1 - 1/n_{Si}^2)} \quad (1)$$

We assume that the absorption coefficient α is composed of $\alpha = \alpha_{bb} + \alpha_{FCA}$ to account for band-to-band transitions and for parasitic absorption of the free carrier plasma, respectively. Thus, the leading factor in eq. (1) selects out of the total absorbance only the fraction that creates electron-hole pairs. The ratio of out-coupled light is defined by $1/n_{Si}^2$, using the refractive index of silicon n_{Si}. Both, α_{bb} and n_{Si} are tabulated for 300 K [17], therefore we use the temperature coefficients given in the same reference to extrapolate them to 298 K. For α_{FCA}, we use a recent parametrisation [18].

The term $T(\alpha w)$ describes the fraction of the transmitted light intensity between two scattering events as illustrated in Fig. 1. Lambertian light scattering is usually associated with a path length enhancement equal to 2. Thus, $T(\alpha w)$ is simply expressed as:

$$T(\alpha w) = \exp(-2\alpha w) \quad (2)$$

Even though frequently used in the literature, eq. (2) is based on the assumption that the Lambertian distribution is maintained at all times. However, in the spectral region where silicon is strongly absorbing, light that is scattered into high angles is absorbed in a shallow region close to the interface whereas light scattered into the specular direction penetrates deeper into the material. Consequently, the angle resolved intensity distribution changes towards a more and more specular profile as illustrated in Fig. 1. Upon scattering at the rear or at the front, the distribution is once again fully randomised. To cover weak as well as strong absorption, $T(\alpha w)$ is expressed with the exponential integral $\mathrm{E_i}(x)$ as follows [19–21]:

$$T(\alpha w) = \exp(-\alpha w) \cdot (1 - \alpha w) + (\alpha w)^2 \mathrm{E_i}(\alpha w) \quad (3)$$

Once the absorptance is defined in terms of $T(\alpha w)$, the photocurrent density j_L is obtained by multiplication with the photon density in the illumination spectrum [22] and numerical integration over the wavelength range of interest. The absorptance gives also access to the probability of photon recycling [8]:

$$P_{PR} = \frac{\int A(\lambda) \cdot B(E) dE}{\int B(E) dE} \quad (4)$$

Here, $B(E)$ is the spectral radiative recombination coefficient [23,24] and we substitute $E = hc/\lambda$ to better comply with tabulated data. Thus, the effect of photon recycling is described by multiplying $(1 - P_{PR,m})$ to the radiative recombination coefficient B that appears in the recombination rate R.

Finally, we model Auger recombination according to a recent parametrisation that takes into account Coulomb-enhancement [6].

Assuming a monolithic tandem structure with an interconnecting

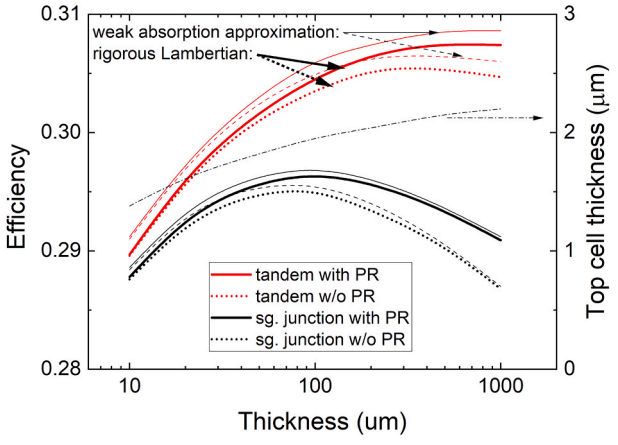

Fig. 2. Limiting efficiencies for Si single-junction (black) and Si/Si tandem solar cells (red) with respect to device thickness. Dashed and full and lines refer to modelling without and with photon recycling, respectively. As indicated by arrows, thin and thick lines represent $T(\alpha w)$ according to eq. (2) and eq. (3), respectively. The dash-dotted curve refers to the top-cell thickness (right scale). (For interpretation of the references to colour in this figure legend, the reader is referred to the Web version of this article.)

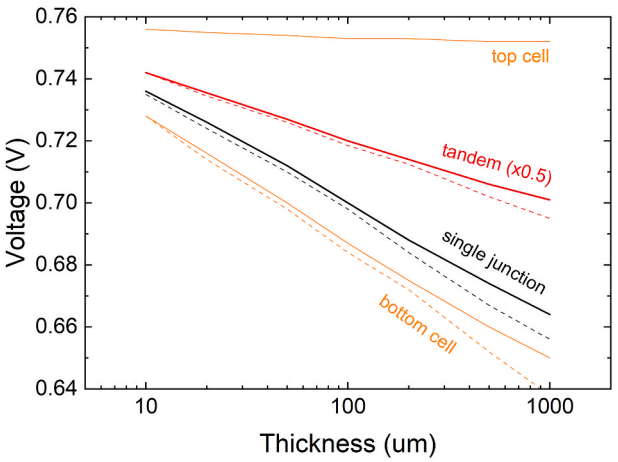

Fig. 3. Voltage at MPP of single junction cells (black) and tandem cells (red, divided by 2 for better illustration). Voltages of the component cells are shown in orange, dashed and full lines refer to modelling without and with photon recycling, respectively. (For interpretation of the references to colour in this figure legend, the reader is referred to the Web version of this article.)

junction made of silicon, light scattering remains unchanged and the infinite sum leading to eq. (1) is readily generalised to express the absorptances in the two stacked component cells ($m = 1, 2$) with their respective thicknesses w_1 and $w_2 = w - w_1$:

$$A_1 = \frac{\alpha_{bb}}{\alpha_{bb} + \alpha_{FCA,1}} \cdot \frac{(1 - T(\alpha_1 w_1)) + T(\alpha_1 w_1 + \alpha_2 w_2)(T(\alpha_2 w_1) - T(\alpha_1 w_1 + \alpha_2 w_2))}{1 - T^2(\alpha_1 w_1 + \alpha_2 w_2)(1 - 1/n_{Si}^2)} \tag{5}$$

$$A_2 = \frac{\alpha_{bb}}{\alpha_{bb} + \alpha_{FCA,2}} \cdot \frac{(T(\alpha_1 w_1) - T(\alpha_1 w_1 + \alpha_2 w_2)) + T(\alpha_1 w_1 + \alpha_2 w_2)(1 - T(\alpha_2 w_2))}{1 - T^2(\alpha_1 w_1 + \alpha_2 w_2)(1 - 1/n_{Si}^2)} \tag{6}$$

After the calculation of R and j_L, the procedure is looped through different bias voltages and the current-voltage characteristic is assembled. In case of the tandem cell, the form $V_m(j)$ is chosen and combined into $V(j) = V_1(j) + V_2(j)$. Subsequently, the maximum of $P(j) = j \cdot V(j)$ is used to find a first approximation for the matched current density and for the voltages at MPP. These are used to adjust Δn and α_{FCA} in the component cells, and another iteration is initiated.

3. Results

The black characteristics in Fig. 2 show projected efficiencies of single junction cells using undoped Si. Using the rigorous treatment of Lambertian scattering according to eq. (3), our implementation predicts a limiting value of 29.63% for a 100 μm thick cell as shown by the thick black line. The numerical value differs slightly from latter 29.56% as found by Schäfer [9], possibly due to differences in the implementation of the models. We note that the simplified transmission factor of eq. (2) overestimates the generation rate; it would yield an efficiency limit 29.68% for 100 μm as indicated by the thin lines in Fig. 2. Finally, the effect of photon recycling is generally assumed minor in silicon solar cells as the indirect bandgap yields a low luminescence efficiency. However, without this effect we obtain a limiting value of only 29.54% instead of 29.63 for the 100 μm thick cell and the difference between the full and the dashed lines in Fig. 2 illustrates that the effect becomes increasingly beneficial as the device thickness increases.

For Si/Si tandems, we find optimum values of 30.53% and 30.74% for the modelling without and with photon recycling, respectively, in both cases for a device thickness of 500 μm. Fig. 2 shows that the simplified Lambertian model according to eq. (2) would yield noticeably higher values. As the overestimation of eq. (2) with respect to eq. (3) is more pronounced for short wavelengths, a lower top-cell thickness would be needed for matching and thus yield higher generation rate.

Table 1
Parameters of the optimum cell configurations without and with the effect of photon recycling. The first four columns are based on the rigorous Lambertian model of eq. (3) and the last two columns refer to an optical model without light scattering in the top cell.

	Single junction		Tandem		Tandem w/o scattering top	
	w/o PR	with PR	w/o PR	with PR	w/o PR	with PR
Thickness (μm)	100	100	2.15/500	2.15/500	4.3/500	
Voc (mV)	762	764	1532	1535	1525	1528
jsc (mA/cm^2)	43.4	43.4	22.3	22.4	22.4	22.4
FF	89.1	89.3	89.4	89.4	88.9	89.3
Efficiency	29.49	29.63	30.53	30.74	30.37	30.56

Fig. 3 illustrates the reason for the gain in the tandem configuration with respect to the single junction cell. Owing to the high level of photogeneration close to the front surface, the top-cell thickness required for current matching varies only between 1.6 and 2.7 μm for the whole range of device thicknesses (between 1.4 and 2.2 μm if eq. (2) is used). Consequently, it maintains a high excess carrier density of ca. 2×10^{16} cm^{-3} and contributes more than 750 mV to the tandem at MPP. In the bottom cell, increasing thickness decreases the carrier density from 1×10^{16} cm^{-3} to 2×10^{15} cm^{-3}. At MPP, it contributes 726 mV in the thinnest tandem, but only 640 mV for the thickest one. Fig. 3 shows that the MPP voltage of the tandem device varies only between 1.48 and 1.39 V whereas the variation in the single-junction cell resembles the strong drop of the bottom cell. The parameters of cells with optimum configuration are summarized in Table 1.

4. Optical model

Silicon solar cells require surface texture to reduce their primary reflection and to enhance the absorption length within the absorber. Usually, textures are obtained by caustic etching of 100-oriented Si which yields square pyramids with 111-oriented facets and a typical size between 2 and 5 μm. Thus, the top-cell should follow the texture conformally at a precisely defined depth and the photocurrent would be created essentially by a single passage of strongly absorbed light. As the photocurrent of the bottom cell is mainly created by weakly absorbed light, we may still assume randomisation of these wavelengths within the remainder of the device [13]. Thus, light scattering in the top-cell should be removed from eqns. (5) and (6), but it should be maintained for the bottom-cell. As a result, the top cell thickness required for current matching is approximately doubled, and its generation rate is reduced accordingly. The limiting efficiencies for the tandem devices are thus reduced by ca. 0.2% (abs) as shown in Table 1. The optical loss could be mitigated by introducing a modulated surface texture that provides scattering for short as well as for long wavelengths [25].

5. Manufacturability

The idea of using same-bandgap tandems is not a new one but was frequently used for a-Si/a-Si tandems made of amorphous silicon solar cells. Initially they were proposed to provide a potential similar to mercury cells [26], e.g. for solar-powered pocket calculators. Soon after, other advantages of same-bandgap tandems were noted [27]. First, the poor transport in a-Si implies a practical limit to the thickness of solar cells that is not sufficient for full absorption of the incident light. Two cells can be stacked to a larger total thickness and thus absorb more light. Second, tandem cells are less vulnerable to light-induced degradation as the strong drift field in the thin top cell maintains good carrier extraction even with the creation of light induced defects during operation. Finally, the a-Si/a-Si tandem cells had a clear advantage for

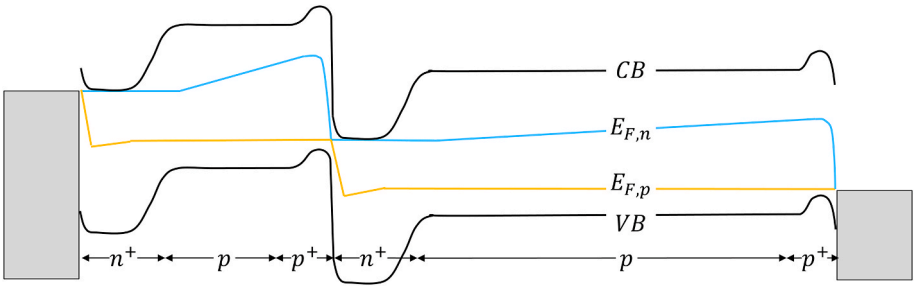

Fig. 4. Schematic band diagram of a monolithic tandem device under operating conditions (illumination and $V < V_{oc}$). Energies and distances not to scale.

module integration as their reduced photocurrent density relaxed the requirement of conductivity in the transparent front contact layer [28,29]. The concept was later extend to the micromorph tandem which covered a wider spectral range by combining different bandgaps in an amorphous top-cell and a nanocrystalline bottom-cell [30].

In the domain of crystalline silicon, c-Si/c-Si tandems could also provide a benefit to module integration. The last years showed a steady increase in wafer size, accompanied by a trend towards module integration of cut cells [31–33]. The reduced current of half, or even smaller, cells requires less silver in the metallisation, but there is a penalty in efficiency because of surface damage along the cleaving edge. The use of c-Si/c-Si tandems would reduce the current without the losses associated to cleaving.

In the monolithic integration that we considered here, the component-cells should be interconnected by a tunnelling-junction between the component-cells, requiring at least four regions with different doping type and concentration. This is well within the capabilities of silicon technology where pn/pn junctions are regularly made with triple-well CMOS processes. Triple-well processes were already used to integrate solar harvesters into self-powered circuits [34,35]. However, the goal of these efforts was not to develop tandem cells but to provide a harvester as add-on to the circuit. Consequently, the dopant profiles were not necessarily ideal for efficient solar cells [34] and only the upper junction was used for a solar cell in single-junction configuration, whereas the underlying junction served to separate the cell from the circuitry [35].

The fabrication of the tunnelling junction would be additionally complicated by the need for surface textures which are mandatory for absorption enhancement in solar cells. Two fabrication methods appear feasible; one could imagine to form a tunnelling junction at the textured surface [36], followed by epitaxy of the top cell and processing of another junction at the front. The issue here would clearly be the epitaxy of a layer with high bulk quality [37], even though the high excess carrier density in the top cell could tolerate a higher level of defect recombination than the bulk of the bottom cell [13]. Alternatively, one could imagine to process the tunnelling junction by deep implantation [38], taking into account the additional complication of implantation into a textured sample surface [39].

Limiting efficiencies are generally calculated by assuming zero losses in the doped regions close to the contacts as well as perfect surface passivation. Here, we assumed the same for the tunnelling junction. Modelling of Si/Si tandem cells with PC1D suggested that the parasitic absorption in these regions remains manageable, but it revealed that there are substantial issues with surface recombination that ultimately limit the gain in operating voltage [40]. Fig. 4 illustrates the issue schematically for the band diagram of a *p*-type tandem solar cell where each of the component-cells contain a highly doped n^+ region at the front and a highly doped p^+-region at the rear. Except for its high doping level, the interconnecting junction is a regular *p-n* junction in which the majority Fermi levels must align. The splitting of the minority Fermi levels cannot extend across the junction as this would indicate occupation of highly excited states that would immediately thermalize to the respective band edges. As a result, the bottom-cell acts for the top-cell like a metallic rear contact with infinite surface recombination velocity and vice-versa. One way to avoid this situation would be the insertion of a passivating oxide layer as demonstrated with passivating tunnelling junctions intended for tandems with perovskite top-cells [41,42]. As the growth of a silicon top-cell on the tunnelling oxide appears challenging, the creation of a buried oxide as in silicon-on-insulator (SOI) technology appears more feasible. Surface recombination velocities between 500 and 1000 cm/s were reported for SOI structures [43], but their use in a Si/Si tandem device would either require contact openings in the oxide [13], and the low refractive index of the oxide would likely violate the assumption of undisturbed light scattering.

Alternatively, a variety of methods was proposed for the fabrication of thin silicon membranes and their processing into solar cells [44,45]. Even though such cells could be contacted completely independently, there are several reasons in favour of a monolithic series connection. For example, applying four contact patterns would cancel the advantage of reduced silver consumption, and misaligned metallisation grids would lead to inacceptable shadowing losses. Moreover, very thin silicon membranes normally require attachment to a carrier substrate for handling [45]. Obviously, a crystalline silicon bottom-cell would be an ideal carrier.

6. Conclusions

We investigated the limiting efficiency of c-Si/c-Si tandem solar cells. Similar to c-Si single-junction solar cells, Auger recombination represents the main limitation. The configuration nevertheless bears an advantage because the top-cell contributes a high voltage due to the high generation rate close to the front surface. For a configuration with ideal Lambertian absorption enhancement, we find an optimum efficiency of 30.74% for a total thickness of 500 μm. This value is surprisingly close to the original estimate of 1986, but it emerges on the basis of different recombination statistics, a different optical model, and for a larger device thickness. The path enhancement in the top-cell is drastically reduced in more realistic cell configurations that employ 111-oriented pyramids at the front. For this case, we estimate that the optimum efficiency can still attain 30.56%. Manufacturing of such devices would require resolving several practical challenges, in particular the one of obtaining a quasi-perfect surface passivation for the buried tunnel junction.

Funding

This work has received funding from the European Union's Horizon 2020 research and innovation programme under grant agreement No 857793.

Credit author statement

FJH developed the idea, carried out the modelling and wrote the manuscript.

Both authors discussed the results.

Declaration of competing interest

The authors declare that they have no known competing financial interests or personal relationships that could have appeared to influence the work reported in this paper.

References

[1] W. Shockley, H.J. Queisser, Detailed balance limit of efficiency of p-n junction solar cells, J. Appl. Phys. 32 (3) (1961) 510–519, https://doi.org/10.1063/1.1736034.

[2] T. Tiedje, E. Yablonovitch, G.D. Cody, B.G. Brooks, Limiting efficiency of silicon solar cells, IEEE Trans. Electron. Dev. 31 (5) (1984) 711–716.

[3] M.J. Kerr, A. Cuevas, General parameterization of Auger recombination in crystalline silicon, J. Appl. Phys. 91 (4) (2002) 2473–2480.

[4] M.J. Kerr, A. Cuevas, P. Campbell, "Limiting efficiency of crystalline silicon solar cells due to Coulomb-enhanced Auger recombination, Prog. Photovoltaics Res. Appl. 11 (2) (2003) 97–104.

[5] R.M. Swanson, "Approaching the 29% Limit Efficiency of Silicon Solar Cells," in Conference Record *of the Thirty-First IEEE Photovoltaic Specialists Conference*, 2005, pp. 889–894, 2005.

[6] A. Richter, S.W. Glunz, F. Werner, J. Schmidt, A. Cuevas, Improved quantitative description of Auger recombination in crystalline silicon, Phys. Rev. B 86 (16) (2012), 165202.

[7] P.P. Altermatt, A. Schenk, F. Geelhaar, G. Heiser, Reassessment of the intrinsic carrier density in crystalline silicon in view of band-gap narrowing, J. Appl. Phys. 93 (3) (2003) 1598–1604.

[8] A. Richter, M. Hermle, S.W. Glunz, Reassessment of the limiting efficiency for crystalline silicon solar cells, IEEE J. Photovolt. 3 (4) (2013) 1184–1191, https://doi.org/10.1109/JPHOTOV.2013.2270351.

[9] S. Schäfer, R. Brendel, Accurate calculation of the absorptance enhances efficiency limit of crystalline silicon solar cells with lambertian light trapping, IEEE J. Photovolt. 8 (4) (2018) 1156–1158.

[10] B.A. Veith-Wolf, S. Schäfer, R. Brendel, J. Schmidt, Reassessment of intrinsic lifetime limit in n-type crystalline silicon and implication on maximum solar cell efficiency, Sol. Energy Mater. Sol. Cells 186 (2018) 194–199.

[11] S. Bhattacharya, S. John, Beyond 30% conversion efficiency in silicon solar cells: a numerical demonstration, Sci. Rep. 9 (1) (2019) 1–15.

[12] U. Strauss, W.W. Rühle, K. Köhler, Auger recombination in intrinsic GaAs, Appl. Phys. Lett. 62 (1) (1993) 55–57.

[13] M.A. Green, Crystalline and polycrystalline silicon tandem junction solar cells: theoretical advantages, Sol. Cell. 18 (1) (1986) 31–40.

[14] M.A. Green, Accuracy of analytical expressions for solar cell fill factors, Sol. Cell. 7 (3) (1982) 337–340.

[15] P.P. Altermatt, F. Geelhaar, T. Trupke, X. Dai, A. Neisser, E. Daub, "Injection Dependence of Spontaneous Radiative Recombination in C-Si: Experiment, Theoretical Analysis, and Simulation," in NUSOD'05. Proceedings of the 5th International Conference on Numerical Simulation of Optoelectronic Devices, 2005, pp. 47–48, 2005.

[16] H.W. Deckman, C.B. Roxlo, E. Yablonovitch, Maximum statistical increase of optical absorption in textured semiconductor films, Opt. Lett. 8 (9) (1983) 491–493.

[17] M.A. Green, Self-consistent optical parameters of intrinsic silicon at 300 K including temperature coefficients, Sol. Energy Mater. Sol. Cells 92 (11) (2008) 1305–1310.

[18] M. Rüdiger, J. Greulich, A. Richter, M. Hermle, Parameterization of free carrier absorption in highly doped silicon for solar cells, IEEE Trans. Electron. Dev. 60 (7) (2013) 2156–2163.

[19] A. Luque, G.L. Araújo, Physical Limitations to Photovoltaic Energy Conversion, Taylor & Francis, 1990.

[20] R. Brendel, M. Hirsch, R. Plieninger, J.H. Werner, Quantum efficiency analysis of thin-layer silicon solar cells with back surface fields and optical confinement, IEEE Trans. Electron. Dev. 43 (7) (1996) 1104–1113.

[21] M.A. Green, "Lambertian light trapping in textured solar cells and light-emitting diodes: analytical solutions, Prog. Photovoltaics Res. Appl. 10 (4) (2002) 235–241.

[22] D. Myers, Review of Consensus Standard Spectra for Flat Plate and Concentrating Photovoltaic Performance, " National Renewable Energy Lab.(NREL), Golden, CO (United States), 2011.

[23] P. Würfel, The chemical potential of radiation, J. Phys. C Solid State Phys. 15 (18) (1982) 3967.

[24] T. Trupke, et al., Temperature dependence of the radiative recombination coefficient of intrinsic crystalline silicon, J. Appl. Phys. 94 (8) (2003) 4930–4937.

[25] A. Ingenito, O. Isabella, M. Zeman, "Nano-cones on micro-pyramids: modulated surface textures for maximal spectral response and high-efficiency solar cells, Prog. Photovoltaics Res. Appl. 23 (11) (2015) 1649–1659.

[26] Y. Hamakawa, H. Okamoto, Y. Nitta, A new type of amorphous silicon photovoltaic cell generating more than 2.0 V, Appl. Phys. Lett. 35 (2) (1979) 187–189.

[27] J.J. Hanak, V. Korsun, "Optical Stability Studies of A-Si: H Solar Cells," in *Proc*, 16th IEEE PVSC, 1982, pp. 1381–1383.

[28] H. Sakai, Y. Ichikawa, Process technology for a-Si/a-Si double stacked tandem solar cells with stabilized 10% efficiency, J. Non-Cryst. Solids 137 (138) (1991) 1155–1160, https://doi.org/10.1016/S0022-3093(05)80328-X.

[29] A. Bubenzer, P. Lechner, H. Schade, H. Rübel, Process technology for mass production of large-area a-Si solar modules, Sol. Energy Mater. Sol. Cells 34 (1–4) (1994) 347–358.

[30] J. Meier, et al., "Towards high-efficiency thin-film silicon solar cells with the 'micromorph' concept, Sol. Energy Mater. Sol. Cells 49 (1–4) (1997) 35–44.

[31] J.D.C. Dickson, Photo-voltaic Semiconductor Apparatus or the like, " US2938938A, 1960.

[32] J. Zhao, A. Wang, E. Abbaspour-Sani, F. Yun, M.A. Green, Improved efficiency silicon solar cell module, IEEE Electron. Device Lett. 18 (2) (Feb. 1997) 48–50, https://doi.org/10.1109/55.553040.

[33] F. Gérenton, et al., Silicon Heterojunction and Half-Cell Configuration: Optimization Path for Increased Module Power, 2019.

[34] B. Sarioglu, O. Aktan, A. Oncu, S. Mutlu, G. Dundar, A.D. Yalcinkaya, An optically powered CMOS receiver system for intravascular magnetic resonance applications, IEEE J. Emerg. Sel. Top. Circuits Syst. 2 (4) (2012) 683–691.

[35] G. Hong, G. Han, Design optimization of photovoltaic cell stacking in a triple-well CMOS process, IEEE Trans. Electron. Dev. 67 (6) (2020) 2381–2385, https://doi.org/10.1109/TED.2020.2986536.

[36] P. Bellanger, A. Minj, A. Fave, Z. Djebbour, S. Roques, A. Slaoui, Silicon tunnel junctions produced by ion implantation and diffusion processes for tandem solar cells, IEEE J. Photovolt. 8 (6) (2018) 1436–1442, https://doi.org/10.1109/JPHOTOV.2018.2864632.

[37] D.K. Schroder, et al., Silicon epitaxial layer recombination and generation lifetime characterization, IEEE Trans. Electron. Dev. 50 (4) (2003) 906–912.

[38] J. Von Borany, B. Schmidt, R. Grötzschel, The application of high energy ion implantation for silicon radiation detectors, Nucl. Instrum. Methods Phys. Res. Sect. Accel. Spectrometers Detect. Assoc. Equip. 377 (2–3) (1996) 514–520.

[39] J. Krügener, F. Kiefer, R. Peibst, H.J. Osten, "Ion Implantation of as, P, B, BF and BF 2 on Planar and Alkaline-Textured Si (001) Surfaces for Photovoltaic Applications," in 2018 22nd International *Conference On Ion Implantation Technology*, IIT), 2018, pp. 90–93.

[40] A. Killam, T. Reblitz, A. Augusto, S. Bowden, "All Silicon Tandem Solar Cell," in, in: IEEE 43rd Photovoltaic Specialists Conference, PVSC), 2016, pp. 2448–2450, 2016.

[41] R. Peibst, et al., From PERC to tandem: POLO-and p+/n+ poly-Si tunneling junction as interface between bottom and top cell, IEEE J. Photovolt. 9 (1) (2018) 49–54.

[42] C. Luderer, C. Reichel, F. Feldmann, M. Bivour, M. Hermle, Passivating and low-resistive poly-Si tunneling junction enabling high-efficiency monolithic perovskite/silicon tandem solar cells, Appl. Phys. Lett. 115 (18) (2019), 182105.

[43] T. Kuwayama, M. Ichimura, E. Arai, Interface recombination velocity of silicon-on-insulator wafers measured by microwave reflectance photoconductivity decay method with electric field, Appl. Phys. Lett. 83 (5) (2003) 928–930.

[44] R. Brendel, Review of layer transfer processes for crystalline thin-film silicon solar cells, Jpn. J. Appl. Phys. 40 (7R) (2001) 4431.

[45] H.S. Radhakrishnan, et al., Improving the quality of epitaxial foils produced using a porous silicon-based layer transfer process for high-efficiency thin-film crystalline silicon solar cells, IEEE J. Photovolt. 4 (1) (2013) 70–77.